Intensity Limits for Propagation of 0.527 μm Laser Beams through Large-Scale-Length Plasmas for Inertial Confinement Fusion

C. Niemann,[1] L. Divol,[1] D. H. Froula,[1] G. Gregori,[1] O. Jones,[1] R. K. Kirkwood,[1] A. J. MacKinnon,[1] N. B. Meezan,[1] J. D. Moody,[1] C. Sorce,[1] L. J. Suter,[1] R. Bahr,[2] W. Seka,[2] and S. H. Glenzer[1]

[1]*Lawrence Livermore National Laboratory, 7000 East Avenue, Livermore, California 94550, USA*
[2]*Laboratory for Laser Energetics, 250 E. River Road, Rochester, New York 14623, USA*
(Received 4 March 2004; published 4 March 2005)

We have established the intensity limits for propagation of a frequency-doubled (2ω, 527 nm) high intensity interaction beam through an underdense large-scale-length plasma. We observe good beam transmission at laser intensities at or below 2×10^{14} W/cm^2 and a strong reduction at intensities up to 10^{15} W/cm^2 due to the onset of parametric scattering instabilities. We show that temporal beam smoothing by spectral dispersion allows a factor of 2 higher intensities while keeping the beam spray constant, which establishes frequency-doubled light as an option for ignition and burn in inertial confinement fusion experiments.

PACS numbers: 52.38.Hb, 52.35.Mw, 52.38.Dx

Indirect-drive inertial confinement fusion in laser facilities such as the National Ignition Facility (NIF) requires a highly symmetric illumination of the hohlraum walls that enclose the ignition capsule [1]. As the laser beams propagate through the gas filled hohlraum, a large-scale-length plasma is formed. Absorption and parametric scattering processes in this plasma reduce the effective laser energy on the hohlraum wall. Plasma induced beam deflection and spray due to self-focusing and filamentation influence the intensity distribution of the laser beams and can have important effects on x-ray drive, capsule symmetry, and hence fusion yield [2,3].

Most previous experiments on laser-plasma interactions related to inertial fusion have concentrated on frequency tripled (of the fundamental 1 μm light of glass lasers) light (3ω, 351 nm) [4–12]. Frequency-doubled light (2ω, 527 nm) is also being explored as a higher gain option for indirect-drive ignition because of the possibility of extracting more laser energy [13,14]. Understanding beam transmission and spray at 2ω is therefore crucial to assess 2ω ignition experiments and to develop predictive laser-plasma interaction capabilities.

In this Letter, we show that temporal beam smoothing by spectral dispersion (SSD) considerably reduces the spray of green (0.527 μm) high intensity laser beam in a large-scale-length laser produced plasma. Angularly resolved beam transmission measurements demonstrate that the intensity can be increased twofold when smoothing by SSD is used. This result suggests possible 2ω laser beam intensities of 4×10^{14} W/cm^2 where backscatter by stimulated Raman scattering (SRS) is moderate of order 10%, making 2ω ignition and burn a realistic option for NIF [13]. We obtain a good quantitative agreement with modeling by a fluid laser-plasma interaction code (pF3d) both in terms of the absolute beam transmission and beam spray, which justifies scaling to NIF.

The experiments were performed at the Omega laser facility [15] using a 2ω interaction beam [16] and the transmitted beam diagnostic (TBD) that was commissioned for the experiments described here. The large-scale-length plasma is created by heating the 2.4 mm by 2.75 mm gasbag target [6] with 39 defocused heater beams at 3ω, delivering a total energy of 10.5 kJ in a 1 ns square pulse. The hydrocarbon gas filling of the gasbag to about 1 atm results in an electron density (n_e) of about 14% of the critical density for 527 nm light ($n_e = 5.5 \times 10^{20}$ cm^{-3}). This corresponds to the current 2ω NIF hohlraum design gas density [13]. The heater beams are distributed in five different cones on both sides of the target in order to provide maximum symmetry. Gated x-ray images of the heated bag and Thomson-scattering measurements show that a homogeneous plasma is formed after a few 100 ps within a blast wave moving inward due to the ablation of the polyimid skin of the bag [17].

The 1 ns long 2ω (527 nm) probe beam has a variable energy between 20 and 400 J and is spatially smoothed with a distributed phase plate giving a vacuum spot diameter of about 200 μm and an intensity up to 10^{15} W/cm^2. The probe beam turns on 500 ps after the start of the heater beams. The beam can further be temporally smoothed by spectral dispersion [18] by applying an oscillating rf field to an electro-optic crystal that modulates the phase of the seed laser pulse. This adds up to 11 Å bandwidth (at 1ω) to the narrow linewidth of the laser which is then dispersed with a grating.

The TBD consists of a fused silica curved 3 in. diameter bare-surface reflector, mounted 23 cm behind the target chamber center (tcc) on a remote controlled diagnostic arm installed in one of the target insertion modules. The mirror collects and reflects transmitted light within twice the f/6.7 cone of the original beam through a window to a detector assembly outside the vacuum chamber (Fig. 1). A second

4% splitter reflects a small fraction of the beam onto a Lambertian diffuser plate, while the remaining beam energy is measured in a full aperture calorimeter filtered for 2ω light (Fig. 1).

Time integrated two-dimensional near-field images of the transmitted light on the diffuser plate are recorded with a CCD camera through a 2ω bandpass filter (10 nm FWHM). The images show the intensity distribution on the mirror behind the target within 8.5° around the beam axis (twice the initial $f/6.7$ cone) and are used to measure beam spray and deflection. A fast photodiode (5 GHz bandwidth) records the temporal pulse shape of the transmitted light at 527 ± 5 nm. All three detectors are absolutely calibrated *in situ* using a low energy (20 J) 2ω laser beam [Fig. 2(a)(III)] to allow independent measurements of the total transmitted energy. The TBD was used in combination with a full aperture backscatter diagnostic and a near backscatter imager which measured stimulated Brillouin and Raman backscattered light into or around the focusing lens.

Figure 2(a) shows the measured near-field images of the interaction beam for various intensities. At an intensity of $\sim 10^{15}$ W/cm^2, the beam exhibits a large spray outside the initial $f/6.7$ cone (dashed inner circle) reaching the edge of the TBD mirror (dotted outer circle). When 11 Å SSD is applied, the beam spray is reduced considerably 2(a)(II). As a reference, Fig. 2(a)(III) shows a low intensity calibration shot without plasma where the beam stays within the $f/6.7$ cone. At an intensity of $\sim 5 \times 10^{14}$ W/cm^2, beam spray is still visible 2(a)(IV). Both 5 and 11 Å SSD provide a similar reduction in spray 2(a)(V). At much lower intensity (1.5×10^{14} W/cm^2), beam spray becomes negligible 2(a)(VI).

Averaged radial intensity profiles [Fig. 2(b)] around the center of the deflected beam quantify the fraction of energy inside a solid angle defined by its half-cone angle φ. Figure 2(c) shows the fraction of transmitted energy inside

the original $f/6.7$ cone as a function of intensity and temporal smoothing. At the highest intensities, only a third of the energy of the unsmoothed beam is contained inside the $f/6.7$ cone. With SSD it increases to 50%, reaching more than 80% for lower intensities (1.5×10^{14} W/cm^2). At high intensities, when the beam spray is large enough to exceed the $f/3.3$ TBD collection mirror, a smooth fit to the wings of the intensity profile is applied to estimate the beam intensity distribution outside the mirror ($\varphi > 8.6°$). For an unsmoothed beam at 10^{15} W/cm^2 roughly 20% of the beam energy is outside the collection mirror. The error bars indicate the variation of beam spray for different directions (horizontal to vertical) due to the asymmetry of the spray. Figure 2(c) shows that, for our plasma conditions, the spray of the 2ω interaction beam is controlled by either reducing its intensity or adding up to 11 Å of SSD bandwidth. Figure 2(a) also shows a small deflection of the beam of the order of 1° to the right.
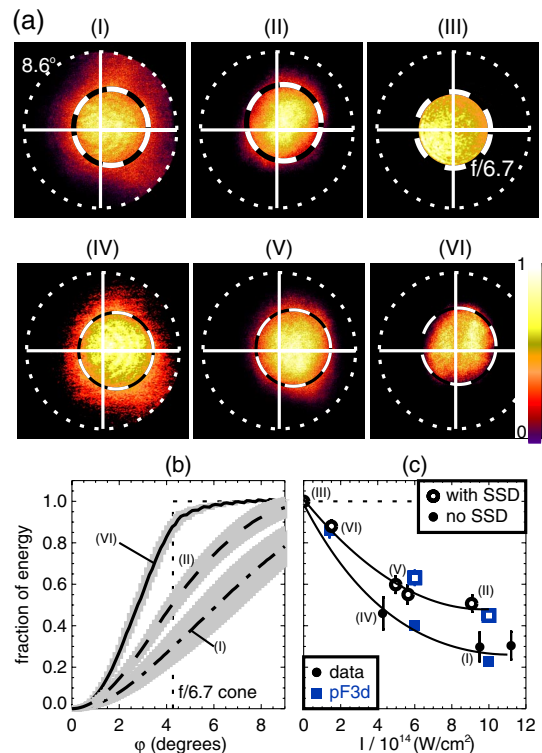
FIG. 2 (color online). (a) Near-field images of a 10^{15} W/cm^2 interaction beam without (I) and with 11 Å SSD (II). (IV) and (V) are the corresponding images for a lower intensity of 5×10^{14} W/cm^2. We also show a low intensity (1.5×10^{14} W/cm^2) shot with 5 Å SSD (VI) and a low energy calibration shot without plasma (III). The cross defines the center of the TBD mirror while the dashed circle represents an $f/6.7$ cone (4.3°) around the transmitted beam centroid. (b) Fraction of beam energy within the angle φ around the beam center corresponding to (I), (II), and (VI). (c) Fraction of energy inside the initial $f/6.7$ cone as a function of beam energy and temporal smoothing and comparison with the modeling. The lines are simple fits to the data.
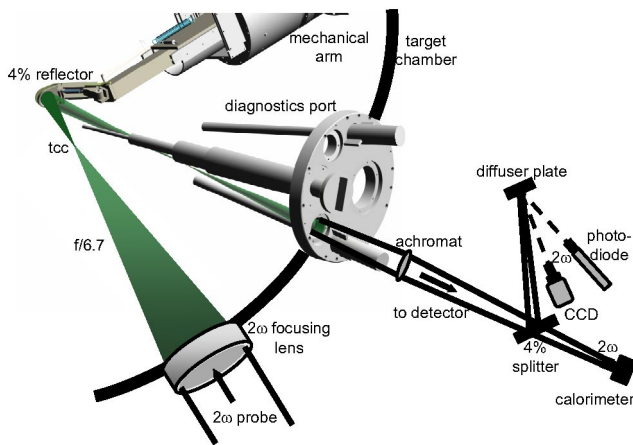

FIG. 1 (color online). Setup of the transmitted beam diagnostic at the Omega target chamber and the mechanical arm that holds the 4% reflector near the target.

Two-dimensional (2D) cylindrical hydrodynamic simulations done with the code HYDRA [19], using a realistic beam pointing and focusing, give the evolution of the plasma density and temperature. A peak electronic temperature $T_e = 1.8$–2 keV is predicted in the 2 mm long density plateau ($n_e \approx 5.5 \times 10^{20}$ cm^{-3}). A simple refraction calculation was used to determine the deflection angle (defined as the angle between the center of the TBD mirror and the beam centroid viewed from tcc),

$$\alpha = \int_{\text{path}} ds \frac{1}{n(s)} \nabla_t n(s), \tag{1}$$

where $n(s)$ is the refractive index along the laser path s and $\nabla_t n(s)$ is the refractivity gradient perpendicular to the path. Using the calculated density profile and the actual interaction beam pointing (offset 200 μm from tcc), Eq. (1) predicts a 1.5° deflection of the beam to the right (in the coordinate system of Fig. 2(a)], in good agreement with the measured deflection between 1° and 1.7° to the right. No additional deflection was observed with increasing intensity, which is consistent with the negligible transverse flow in these targets [20].

Hydrodynamic profiles at 0.8 and 1.2 ns (the interaction beam is on from 0.5 to 1.5 ns) were used as input for more detailed laser-plasma interaction simulations, using pF3d [21]. The calculations include a coupled-wave model of backscattering instabilities with a nonlinear hydrodynamic module and a model for nonlocal heat conduction [21]. Ponderomotive and thermal filamentation are thus naturally present, driving density perturbations resulting in refraction, diffraction, and beam spray. The simulations were done in a 2D planar geometry, using the measured focal spot shape and a realistic model of spatial and temporal smoothing.

The calculated beam spray is shown in Fig. 2(c). The error bars correspond to the uncertainty in plasma parameters from the HYDRA simulations (by comparing various heat conduction models) and their evolution between 0.8 and 1.2 ns. The threshold and the increase in beam spray with intensity are well reproduced, as well as the strong beneficial effect of temporal smoothing.

Figure 3 shows the propagation of the interaction beam through the plasma. Most of the filamentation and spray occurs in the blast wave first traversed by the interaction beam, about $z = 0.7$ mm. In this short (200 μm) and dense ($n_e \approx 10^{21}$ cm^{-3}) [Fig. 3(a)] plasma, a significant fraction of the speckles generated by the phase plate are above their critical power for self-focusing when the average intensity reaches $(2$–$3) \times 10^{14}$ W/cm^{-2}, consistent with the onset of beam spray seen in Fig. 2(c).

Thermal filamentation contributes also to the beam spray. A simulation where thermal effects are turned off and only ponderomotive filamentation is considered [with laser parameters corresponding to Fig. 2(a)(IV)] shows 50% of the energy inside the f/6.7 cone versus 40%
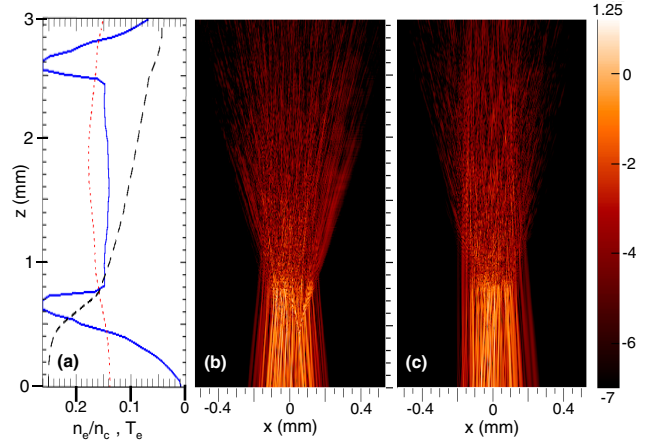

FIG. 3 (color online). Beam propagation simulated by pF3d at an intensity of 6×10^{14} W/cm^2 without (b) and with 11 Å of SSD (c). The color bar units are $\log(I/I_0)$, where I_0 is the average beam intensity. Also shown in (a) are the calculated n_e/n_c (solid line), T_e (dotted, in units of 10 keV), together with the corresponding absorption of the beam by inverse bremsstrahlung (dashed, arbitrary units).

when thermal effects are included. Indeed, the electron mean free path in the blast wave is $\lambda_{ei} \approx 8$ μm, comparable to a speckle width $2f\lambda_0 = 6$ μm, which suggests that heat conduction will not smooth out temperature (and therefore density) perturbations. It should be noted that, at the highest intensity, the maximum local temperature perturbation reaches $\delta T_e/T_e = 0.35$, certainly close to the limit of validity for pF3d's (linear) nonlocal heat conduction model. Also, these 2D simulations could overestimate the beam spray, as the lost transverse degree of freedom leads to larger density and temperature perturbations. A multiplier on the local intensity is used to recover the correct average intensity as the beam propagates [i.e., reproducing the three dimensional (3D) Rayleigh length]. As the critical power for ponderomotive filamentation of a speckle is the same (within 20%) in 2D or 3D [22], we expect good agreement between our 2D modeling and measurements done near the filamentation threshold (4×10^{14} W/cm^{-2}). As three dimensional simulations of these large targets are not practical with current computers, simulation results at higher intensity are our best estimate but could be different in 3D.

In order to assess the efficiency of SSD in reducing beam spray, we estimate the time a speckle needs to create a density hole to be the transit time of an ion acoustic wave traveling at the speed of sound ($c_s = [(ZT_e + 3T_i)/M]^{1/2} \approx 0.4$ μm ps^{-1} for our plasma conditions, where T_i is the ion temperature, Z the ion charge state, and M its mass) through an f/6.7 speckle $T_{\text{trans}} = f\lambda_0/C_s \approx 9$ ps. This can be compared with the lifetime of a speckle, given by the laser correlation time $T_{\text{corr}} = 2\pi/\Delta\omega_{\text{ssd}} = 3.4(1.7)$ ps for 5 (11) Å of SSD bandwidth at 1.053 μm. This is consistent with the strong reduction of beam spray mea-
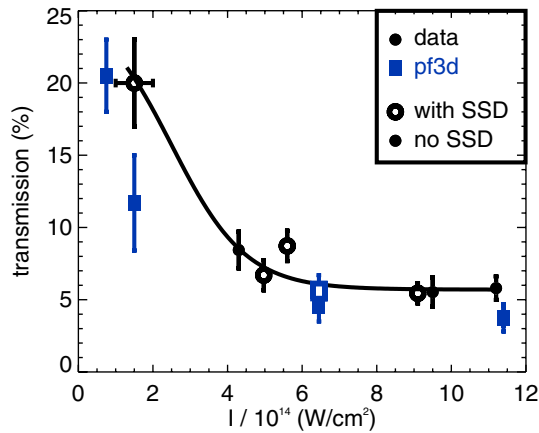
FIG. 4 (color online). Measured beam transmission as a function of intensity with and without SSD (circles) and comparison with pf3d calculations (boxes).

sured when several Å of SSD bandwidth are used as T_{corr} becomes much shorter than T_{trans}.

Besides beam spray, the TBD measures the absolute interaction beam transmission. It decreases with intensity from ~20% at 1.5×10^{14} W/cm² to ~6% at 10^{15} W/cm² (Fig. 4). The error bars indicate the variation of experimental results obtained independently with the calorimeter, the diode, and the CCD camera, and include the intrinsic precision of each instrument. We find that the measured transmitted energy fraction of the 2ω beam is independent of SSD. The (time-averaged) inverse bremsstrahlung absorption calculated with HYDRA is ≈ 0.75–0.85, in agreement with the measured transmission at low intensity. Figure 4 shows that pF3d also reproduces the decrease of the transmission with increasing intensity. This is due to SRS originating from the density plateau, of up to 30% for the highest intensity. The SRS threshold is found at about 10^{14} W/cm⁻², leading to the large error of 30% in the calculated transmission around this intensity.

The full aperture backscatter measurements of Brillouin and Raman backscattered light show only $\leq 10\%$ SRS as strong reabsorption occurs in the blast wave. This is well below the peak 30% SRS seen in simulations in the density plateau. For the low intensity of ~10^{14} W/cm², measured backscatter levels of $\leq 5\%$ SRS and a beam transmission of ~20% suggest good laser coupling for 2ω ignition hohlraum targets. While SSD strongly reduces the beam spray, it only marginally affects SRS, as the instability develops on a much faster time scale (<1 ps) than filamentation (≈ 10 ps). At the highest intensities of

about 10^{15} W/cm² where the beam spray is large enough to exceed the f/3.3 TBD collection mirror the total beam transmission can be up to 20% higher than the measured value, which is within the error bars of the measurement.

In summary, we have shown that the spray of the 2ω interaction beam in an ignition scale plasma is controlled by reducing its intensity to a few times 10^{14} W/cm⁻². Adding up to 11 Å of SSD bandwidth allows a factor of 2 higher intensities while keeping the beam spray constant. Our fluid laser-plasma interaction modeling is in good agreement with these results, which justifies the scaling to NIF conditions. This suggests that future experiments using 527 nm light and large-scale plasmas where beam propagation is critical should stay in this range of intensities.

[1] J. Lindl, Phys. Plasmas **2**, 3933 (1995).
[2] R. L. Kauffman *et al.*, Phys. Rev. Lett. **73**, 2320 (1994).
[3] J. D. Moody *et al.*, Phys. Rev. Lett. **83**, 1783 (1999).
[4] W. Seka *et al.*, Phys. Fluids B **4**, 2232 (1992).
[5] H. A. Baldis *et al.*, Phys. Fluids B **3**, 2341 (1991).
[6] B. J. MacGowan *et al.*, Phys. Plasmas **3**, 2029 (1996).
[7] J. C. Fernández *et al.*, Phys. Plasmas **4**, 1849 (1997).
[8] D. S. Montgomery *et al.*, Phys. Plasmas **5**, 1973 (1998).
[9] S. H. Glenzer *et al.*, Phys. Rev. Lett. **80**, 2845 (1998).
[10] J. C. Fernández *et al.*, Phys. Rev. Lett. **81**, 2252 (1998).
[11] J. D. Moody *et al.*, Phys. Plasmas **7**, 3388 (2000).
[12] R. K. Kirkwood *et al.*, Phys. Plasmas **10**, 2948 (2003).
[13] L. J. Suter *et al.*, Phys. Plasmas **11**, 2738 (2004).
[14] M. Stevenson *et al.*, Phys. Plasmas **11**, 2709 (2004).
[15] J. M. Sources *et al.*, Fusion Technol. **30**, 492 (1996).
[16] A. J. Mackinnon *et al.*, Rev. Sci. Instrum. **75**, 3906 (2004).
[17] S. H. Glenzer *et al.*, Phys. Rev. E **55**, 927 (1997); S. H. Glenzer *et al.*, *ibid.* **62**, 2728 (2000).
[18] S. Skupsky *et al.*, J. Appl. Phys. **66**, 3456 (1989).
[19] M. Marinak *et al.*, Phys. Plasmas **5**, 1125 (1998).
[20] H. A. Rose *et al.*, Phys. Plasmas **3**, 1709 (1996).
[21] R. L. Berger *et al.*, Phys. Plasmas **5**, 4337 (1998).
[22] A. V. Maximov *et al.*, Phys. Plasmas **8**, 1319 (2001).